NOVA: Navigation Optimization via UWB-Assisted Iterative Path Planning for UAV Delivery

Dokyun Ryoo[1], Yongjae Yoo[2], Jeongyeup Paek[3], and Saewoong Bahk[1]

[1]Department of Electrical and Computer Engineering and INMC, Seoul National University, Seoul, Republic of Korea
[2]Samsung Electronics Co. Ltd, Repulbic of Korea
[3]Department of Computer Science and Engineering, Chung-Ang University, Seoul, Republic of Korea

***Abstract*—Emerging drone delivery systems face challenges in last-meter package deployment due to positioning inaccuracies of GPS. Ultra-wideband (UWB) technology offers high-precision ranging, and when combined with IMU-based dead reckoning, it can enhance drone navigation to enable precise arrival at the destination. However, drone-to-tag UWB localization presents several challenges, including *flip ambiguity*, *IMU drift*, and *horizontal insensitivity* due to high-altitude flights. To address the challenges, we propose *NOVA*, a navigation optimization scheme via UWB-assisted iterative path planning. With *NOVA*, the drone follows a trajectory that mitigates flip ambiguity while an iterative joint optimization process simultaneously estimates the UWB tag's position and refines the drone's trajectory. At the vicinity of the tag, the drone performs subtle 2D corrective maneuvers during descent to ensure precise last-meter positioning. We evaluate *NOVA* via real experiments and simulations, demonstrating an average navigation error of 0.83 m with 25.45% trajectory overhead.**

I. Introduction

Interest in drone-based package delivery is rapidly expanding and shaping the future of next-generation logistics. The global drone package delivery market is projected to grow from $693 million in 2024 to $4.67 billion by 2030, with a compound annual growth rate of 37.4% [1]. This growth is driven by the efficiency of aerial transportation compared to traditional road-based logistics. By bypassing ground traffic, drones enable rapid deliveries in urban areas without being affected by congestion, and support operations in remote or disaster-affected regions where existing infrastructure may be unreliable or unavailable [2], [3].

Despite the rapid growth of drone delivery, the last-meter approach–the precise landing and package handoff–remains a critical challenge. Reliable last-meter delivery requires precise localization accuracy ($\leq$1.5 meter) [4], yet existing solutions fall short of this requirement. Current approaches such as dropping packages near the destination [5] or relying solely on RF [6] or GPS-based positioning [7] often suffer from high localization errors, leading to unreliable deliveries. Conversely, high-precision solutions such as acoustic-based landing systems [8] or dedicated landing stations require additional infrastructure, increasing deployment cost [9], while vision-based systems introduce privacy concerns [10] and demand high computational resources [11]. These challenges underscore the need for an infrastructure-free, high-accuracy localization approach that enables precise last-meter delivery without relying on external landing aids or human intervention.

This research was conducted under the supervision of the IITP (Institute for Information & Communications Technology Planning & Evaluation) with the support of the MSIT (Ministry of Science and ICT) by the research funds from IITP (Project Numbers: IITP-2026-2021-002048, IITP-2026-RS-2024-00405128, IITP-2026-RS-2024-00398157).

Saewoong Bahk is the corresponding author. (sbahk@snu.ac.kr)

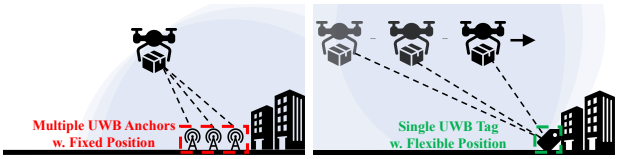

(a) UWB localization based on multiple fixed anchors. **(b)** UWB localization based on a single mobile anchor.

Fig. 1: UWB localization scenarios.

Ultra-wideband (UWB) technology, with its centimeter-level ranging accuracy, presents a promising solution for high-precision localization [12]. To enable UWB localization without pre-installed anchors, we propose a drone-driven approach where a single moving drone, acting as multiple *virtual anchors* at different positions, continuously refines the estimated position of the UWB tag through sequential ranging measurements.

However, localization based on a single mobile anchor also has several technical challenges. First, *flip ambiguity* arises from the symmetric nature of distance measurements, causing the drone to misinterpret its approach direction. While trajectory variation can help resolve this issue, it increases flight distance, creating a trade-off between accuracy and efficiency. Second, *compounded errors from ambiguous drone positioning* arise as the drone acts as both a navigator and a mobile anchor. Last-meter delivery requires solving two interdependent problems: (1) localize itself in 3D space, and (2) use that estimate to guide its UWB tag localization. Any error in self-localization estimate–such as drift from inertial navigation system (INS)–directly corrupts the tag estimate, which in turn steers the drone in the wrong direction, amplifying errors through a reinforcing feedback loop. Lastly, *horizontal localization insensitivity problem*, caused by a dominant Z-component in high-altitude flight, reduces the effectiveness of drone movement in refining position estimates, making precise localization more challenging.

To address the challenges, we propose *NOVA*, a navigation optimization scheme via UWB-assisted iterative path planning

for accurate and reliable drone delivery. The dilution of precision (DOP)-based trajectory planning optimizes waypoints by computing a weighted sum of DOP and normalized distances. This allows efficient navigation while mitigating flip ambiguity by introducing sufficient trajectory variation to prevent incorrect approach directions. Upon reaching each waypoint, the joint optimization process refines both the drone's trajectory and the UWB tag's estimated position to address ambiguity caused by sensor measurement errors.

The drone's trajectory is corrected using a reliability-based exponential moving average (EMA) filter, which compensates for drifts by leveraging the difference between IMU-derived velocity and UWB ranging measurements. Additionally, a gradient descent-based multilateration improves the UWB tag's position estimate using the corrected trajectory and distance measurements. Finally, as the drone approaches the estimated UWB tag position, it initiates a descent process with small corrective movements to compensate for the horizontal localization error caused by high-altitude flight. During this phase, it continuously refines the drone-UWB relative positioning to achieve precise localization, despite the reduced distance variation in the horizontal plane before final touchdown.

Our main contributions are summarized as follows:

- We identify key challenges that arise single-tag UWB localization from a drone, including flip ambiguity, positioning ambiguity, and horizontal localization sensitivity problems.
- We propose *NOVA*, a navigation optimization scheme that resolves the aforementioned challenges via iterative path planning and UWB-assisted localization.
- We implement *NOVA* and evaluate via real experiments and simulations to demonstrate that *NOVA* significantly improves both localization accuracy and trajectory efficiency.

The remainder of the paper: We review prior work in §II, and motivate our work in §III. We propose *NOVA* in §IV, evaluate in §V, and conclude the paper in §VI.

II. Related Work

This section reviews prior work on localization and navigation of drone, also known as unmanned aerial vehicle (UAV), with a focus on last-meter delivery.

A. UAV Localization

GNSS-based methods have been the dominant solution for UAV navigation, offering meter-level accuracy in open areas [13], but suffer in complex environments due to occlusion and multipath [14]. Research on GNSS enhancements, including DGPS [15], RTK [16], and GPS mirror techniques [14], have improved positioning precision in constrained environments, with RTK achieving centimeter-level accuracy under ideal conditions. However, these methods rely on fixed infrastructure and pre-mapped environments, limiting their scalability in real-world UAV deployments.

To overcome GNSS limitations, vision-based methods such as SLAM, visual odometry (VO), and visual-inertial odometry (VIO) have been explored [17], [18], [19], offering strong performance in structured settings. However, they remain sensitive to lighting, occlusion, and privacy issues. RF-based alternatives like BLE [20], Wi-Fi [21], mmWave [22] can achieve sub-meter accuracy, but face challenges with multipath and require dense infrastructure. Non-visual fusion using LiDAR [23], ultrasound [24], or barometric sensors [25] reduce IMU drift, though with high hardware or computation cost.

UWB localization is well-suited for UAVs, offering high accuracy, low latency, and robustness to multipath interference [26]. Multi-anchor systems use multiple fixed nodes [26], but require synchronized clocks, calibration, and infrastructure. To overcome these limitations, recent work has explored single-anchor UWB, where a UAV localizes itself over time by combining range-only UWB measurements with the known position of a stationary anchor. Luo et al.[27] combined VIO with UWB but remained vision-dependent. Zhou et al.[28] performed 2D tracking with fused odometry and UWB, while Cao et al. [29] proposed tightly coupled IMU-UWB fusion to mitigate drift, though both approaches assume planar motion or strong initialization.

More recent research has explored anchor-free relative positioning, where UAVs estimate each other's location using mutual UWB-IMU observations without fixed references. Bao et al. [30] used an MLP to learn UWB-IMU fusion, while Wang et al. [31] introduced DREM-based estimation without persistent excitation, and Lv et al. [32] proposed an adaptive CKF for variable noise. However, these methods often require diverse motion, offline training, or remain unvalidated in real UAV experiments. In contrast, our method targets infrastructure-free deployment with explicit consideration for drift, vertical observability, and poor initialization–gaps left open by prior work.

B. UAV Last-Meter Delivery System

UAV navigation for last-meter delivery is particularly challenged by cluttered environments, occlusions, and unreliable GNSS signals in urban settings. Hybrid GPS-vision systems combine global positioning with visual markers, such as WhyCon [33], or detect fixed physical patterns using object recognition [34] to support precision landing. While effective in controlled settings, these methods require pre-installed infrastructure and are vulnerable to occlusion. To reduce dependence on physical markers, semantic vision and SLAM have been employed to identify landing zones like doors or yards [35], though they suffer from ambiguity in visually complex environments. Learning-based approaches [11] show promise in cluttered 3D spaces, but require large datasets and high computation. Ultimately, all of these approaches depend on visual cues, which can fail in low-light or obstructed conditions. In contrast, our method relies on UWB and inertial data to enable robust, infrastructure-free localization under challenging real-world conditions.

III. Problem Formulation

We introduce the last-meter delivery problem and outline key challenges: flip ambiguity, compound errors in UAV positioning, and error propagation in horizontal localization.

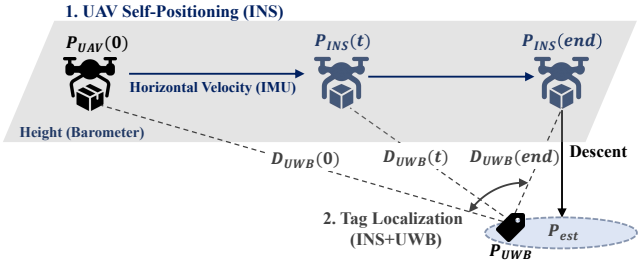

Fig. 2: UAV-based single-tag localization & navigation.

A. Single UWB Tag Localization & Navigation Model

We aim to enable UAV-based package delivery to a location marked by a single UWB tag (Fig. 1(b)). The tag remains stationary at the target location, and it is the goal of the UAV to estimate the tag's position in real-time during the flight. Initially, the UAV navigates using GPS, but transitions to INS- and UWB-based localization for precise last-meter navigation once reliable UWB signals are detected.

Fig. 2 illustrates the overall problem of localizing and navigating toward a single UWB tag from a UAV. This problem consists of two tightly coupled components: (1) the UAV must accurately localize itself in 3D space using onboard sensors, and (2) it must infer the position of the UWB tag from range-only measurements. The UAV estimates its position using INS data, which fuses measurements from the IMU sensors and barometer. 3D acceleration measurements are integrated to estimate the UAV's velocity, in which we focus on the horizontal components $v_x(t)$ and $v_y(t)$. For vertical displacement, we use barometric altitude $h_{\text{barometer}}(t)$ as it offers greater reliability than IMU-based estimates. Combining the horizontal velocity and barometric altitude, the UAV's estimated position at time t, denoted $p_{\text{INS}}(t)$, is expressed as:

$$p_{\text{INS}}(t) = \left(\int v_x(t)\, dt,\ \int v_y(t)\, dt,\ h_{\text{barometer}}(t) \right). \tag{1}$$

With its position estimated via INS, the UAV localizes the UWB tag by combining its estimated trajectory with UWB ranging measurements. Let $D_{\text{3D}}(t)$ represent the true 3D distance between the UAV and the tag; this satisfies the following geometric constraint:

$$\|p_{\text{UAV}}(t) - p_{\text{tag}}\| = D_{\text{3D}}(t) \tag{2}$$

where $p_{\text{UAV}}(t)$ and p_{tag} denote the ground truth positions of UAV at time t and UWB, respectively.

The actual UWB range measurement $D_{\text{UWB}}(t)$ deviates from this true value due to measurement noise:

$$D_{\text{UWB}}(t) = D_{\text{3D}}(t) + \epsilon_d, \tag{3}$$

where ϵ_d represents UWB measurement noise. Since $D_{\text{3D}}(t)$ is unknown, the UAV must estimate the tag's position by minimizing the inconsistency across multiple measurements.

At each time step t, the UAV obtains a UWB range measurement, defining a sphere centered at $p_{\text{INS}}(t)$ with radius $D_{\text{UWB}}(t)$. With three or more such spheres from distinct positions, the UWB tag's position can be estimated through multilateration. To refine the estimated UWB tag position $\hat{p}_{\text{tag}}$, we minimize the Mean Squared Error (MSE) between the predicted and measured distances:

$$\hat{p}_{\text{tag}} = \arg\min_{p} \sum_{t} \left(\|p - p_{\text{INS}}(t)\| - D_{\text{UWB}}(t) \right)^2. \tag{4}$$

As new measurements are acquired, this iterative process refines $\hat{p}_{\text{tag}}$, improving localization accuracy, and the UAV follows the shortest horizontal 2D path toward $\hat{p}_{\text{tag}}$ before executing a final vertical maneuver—either descending or ascending—to precisely reach the target altitude.

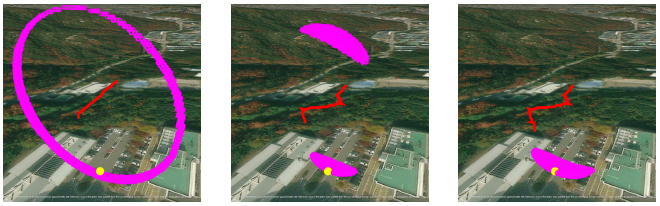

(a) Flip ambiguity in a straight-line UAV trajectory. **(b)** Flip ambiguity in a laterally oscillating UAV trajectory. **(c)** Flip ambiguity resolution via lateral and vertical UAV trajectory.

Fig. 3: Visualization of flip ambiguity in single-anchor UWB localization. The UAV trajectory (red) and true UWB tag position (yellow) are overlaid with high-confidence samples (magenta).

B. Flip Ambiguity

Flip ambiguity is a fundamental challenge in single-anchor UWB localization, where the observer (i.e. UAV) cannot inherently distinguish between two opposite directions due to the nature of distance measurements [36]. Unlike multi-anchor systems, single-anchor systems provide only a scalar distance, placing the UAV on a 3D sphere relative to the tag. This symmetry leads to multiple possible positions satisfying the same distance constraint, making location estimate ambiguous.

The nature of UAV motion further exacerbates this challenge. UAVs typically follow straight-line trajectories, especially when navigating toward a target. When combined with scalar-only UWB distance measurements, this trajectory lacks sufficient geometric diversity to resolve the UAV's orientation relative to the UWB tag. As a result, flip ambiguity extends beyond a single incorrect position to an entire set of indistinguishable candidate locations along the perpendicular bisector of the UAV's trajectory.

Fig. 3 depicts the effect of flip ambiguity in single-anchor UWB localization using real UAV flight data[1]. In Fig. 3(a), a 30 m straight-line trajectory leads to a circular ambiguity pattern, as the intersection of range spheres forms a ring of plausible positions. Fig. 3(b) shows that adding lateral oscillations (±5m side movement) introduces geometric diversity and reduces ambiguity, though vertical uncertainty remains. Fig. 3(c) demonstrates that incorporating vertical motion (5 m descent) resolves the ambiguity entirely. These results highlight a fundamental trade-off: while further trajectory variation may improve localization accuracy, it conflicts with the goal of minimizing flight time and ensuring fast UAV delivery.

[1]Top 2,000 candidates with the lowest loss from Eq. (4), selected from a $200 \times 200 \times 200$ m grid discretized at 0.5 m resolution.

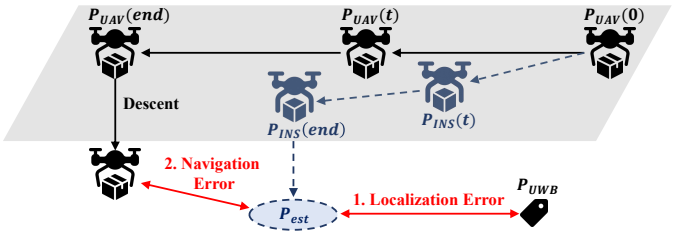

Fig. 4: Compounded errors from UAV ambiguity.

TABLE I: Error under different IMU configurations. The UAV flies 30 m with ±5 m lateral motion in a flip-ambiguity-free scenario. Simulation parameters are described in §V.

Case	Configuration	Error (m)
1	GT UAV + GT Distance	1.59e-9
2	INS UAV + UWB Distance (Localization Only)	2.40
3	INS UAV + UWB Distance + Navigation	5.41

C. Compound Errors from Ambiguous Drone Position

IMU drift is a well-known challenge in INS, where small errors in acceleration and angular velocity accumulate over time through integration [37]. Without external correction, these errors gradually lead to deviation from the ground-truth. Moreover, UAVs are inherently susceptible to short-term disturbances–such as wind and control latency–that further degrade the robustness of their estimated position [38]. In our scenario, this drift introduces a dual challenge: It affects both the UAV's self-localization and the accuracy of multilateration-based UWB tag estimation. Since UWB tag localization relies on the UAV's position as a reference, drift directly corrupts tag estimates—even sub-meter UWB noise becomes problematic when combined with a drifting UAV. Moreover, when the UAV navigates using its own erroneous estimate, the compounded error drives it away from the true tag position, as both localization and control are anchored to incorrect information.

To demonstrate the effect of IMU drift, we compare three simulation cases summarized in Table I. Case 1 uses ground-truth UAV positions and distances for ideal multilateration, yielding negligible error. In Case 2, the UAV localizes the tag using UWB ranges and its INS-estimated trajectory, revealing the impact of drift on its role as a reference anchor. Case 3 includes both localization and navigation based on the its own drifted state, further amplifying the error due to compounded uncertainty in both steps. These results highlight the dual impact of IMU drift: it degrades both the estimated anchor (UAV) and the inferred target (UWB tag), making accurate last-meter positioning extremely difficult to achieve.

D. 3D Error Propagation in Horizontal Localization

In UAV-based UWB tag localization, the UAV's altitude significantly affects horizontal accuracy. As it maintains a fixed height and approaches the UWB tag, the vertical gap $\Delta H(t)$ becomes the dominant component in the 3D distance, amplifying the impact of UWB noise on horizontal localization. To analyze this effect, we decompose the distance $D_{3D}(t)$ between the UAV and UWB tag into its horizontal and vertical components. The 2D distance $D_{2D}(t)$ is given by:

$$D_{2D}(t) = \sqrt{D_{3D}^2(t) - \Delta H^2(t)}. \tag{5}$$

Differentiating both sides of Eq. (5) with respect to $D_{3D}(t)$:

$$\frac{dD_{2D}}{dD_{3D}} = \frac{1}{2} \cdot \frac{2D_{3D}}{\sqrt{D_{3D}^2 - \Delta H^2}} = \frac{D_{3D}}{D_{2D}} = \frac{\sqrt{D_{2D}^2 + \Delta H^2}}{D_{2D}} \tag{6}$$

Eq. (6) shows that the sensitivity of horizontal distance to UWB range measurements depends on the ratio $\Delta H / D_{2D}$. As the UAV approaches the tag at a fixed altitude, the nearly constant $\Delta H(t)$ combined with a decreasing D_{2D} increases the ratio, thereby amplifying the effect of UWB measurement noise on horizontal localization. Given a small perturbation ϵ_d in Eq. (3), the corresponding horizontal localization error propagates as:

$$\Delta D_{2D} \approx \frac{\sqrt{D_{2D}^2 + \Delta H^2}}{D_{2D}} \epsilon_d. \tag{7}$$

Eq. (7) shows that as the UAV approaches the tag while maintaining a fixed altitude, noise amplification increases due to a growing ratio $\Delta H / D_{2D}$. This imposes a fundamental constraint on last-meter accuracy, especially when $D_{2D} \ll \Delta H$. Fig. 5 visualizes how UWB noise propagates through this mechanism as a function of the distance ratio. Assuming a system-level ranging error of 0.28 m [39], achieving 1 m and 1.5 m accuracy requires ratios of at least 0.28 and 0.186, respectively. At a UAV altitude of 30 m, this corresponds to minimum horizontal distances of 8.75 m and 5.68 m—well beyond typical last-meter ranges—highlighting a key limitation of high-altitude UWB-based localization.

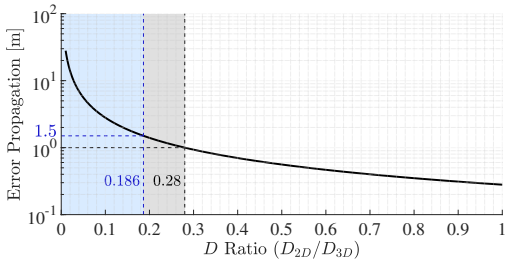

Fig. 5: Approximated horizontal localization error as a function of the distance ratio D_{2D}/D_{3D}.

IV. Proposed Framework: *NOVA*

This section presents *NOVA* that enables precise last-meter drone navigation using a single UWB tag. As depicted in Fig. 6, *NOVA* begins with an *Initial Phase* that collects distinct sensor measurements through vertical and lateral motion to generate a coarse estimate of the tag position. The *Mid-Flight Phase* then iteratively refines both the UAV trajectory and tag estimate through a closed loop of DOP-based planning and joint optimization, continuing until the UAV reaches a predefined proximity threshold. Finally, the *Final Phase* performs a two-step descent to achieve high-precision arrival in close proximity to the tag.

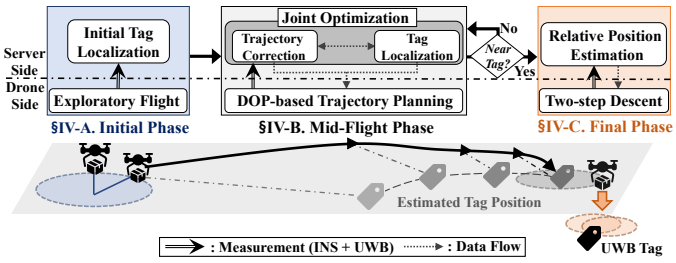

Fig. 6: Overview of *NOVA*.

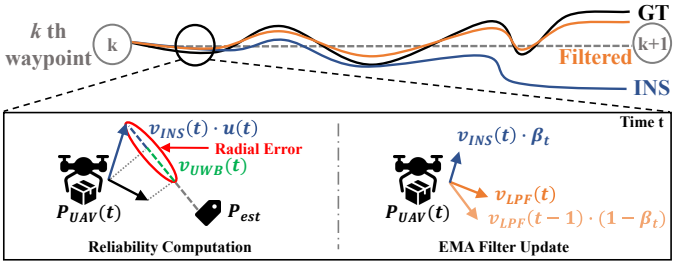

Fig. 7: Concept of reliability based EMA Filter.

A. Initial Phase

Robust 3D localization relies on gathering measurements along all spatial dimensions. A purely planar flight, however, lacks vertical (z-axis) variation, which can lead to significant errors in altitude estimation and consequently degrade overall localization accuracy. To address this, the UAV performs an *exploratory flight* that enhances spatial diversity by combining vertical and horizontal motion. Specifically, the UAV first descends vertically by z_{init} meters to acquire altitude information, then transitions to a horizontal flight over distance D_{init} in a direction orthogonal to the estimated tag location.

This flight configuration is motivated by the Fisher Information Matrix (FIM), which quantifies the amount of information available for estimating the tag's position. In particular, when measurements are taken from two positions separated by an angle α with respect to the true tag, the determinant of the FIM is proportional to $\sin^2 \alpha$. This implies that a trajectory orthogonal to the tag direction ($\alpha = 90°$) maximizes localization information. While the actual tag location is unknown, flying orthogonal to the estimated direction serves as an effective approximation of this optimal condition to enhance geometric diversity and enriches the dataset for reliable 3D estimation.

Throughout this exploratory flight, the UAV collects synchronized IMU, barometric, and UWB measurements to reconstruct its trajectory. A coarse tag estimate is then computed via multilateration, forming the geometric baseline for the iterative refinement process in the mid-flight phase.

B. Mid-Flight Phase – DOP-based Trajectory Planning

Mid-flight phase incrementally refines the UAV's trajectory and the UWB tag position through an iterative pipeline composed of two tightly coupled modules: *DOP-based Trajectory Planning* (§IV-B) and *Joint Optimization* (§IV-C). The former selects informative next waypoints by balancing geometric diversity and travel efficiency, while the latter jointly refines the UAV trajectory and tag estimate using UWB and inertial measurements.

At each iteration, the DOP-based trajectory plannner constructs a set $\mathcal{S}$ of candidate positions, evenly distributed on a circle centered at the current UAV location p_{curr}, with radius $d = \frac{1}{2}\|p^{xy}_{\text{curr}} - \hat{p}^{xy}_{\text{tag}}\|$ and angular resolution $2\pi/n$, where p^{xy} denotes the horizontal projection of a 3D vector p.

The next waypoint is selected as the candidate $p \in \mathcal{S}$ with the lowest cost:

$$\mathcal{L}(p) = \lambda \cdot \underbrace{\frac{\|p - \hat{p}_{\text{tag}}\|}{\|p_{\text{curr}} - \hat{p}_{\text{tag}}\|}}_{\text{Normalized travel cost}} + (1-\lambda) \cdot \underbrace{\text{HDOP}(\mathcal{P}_{\text{UAV}} \cup \{p\})}_{\text{Expected localization gain}}. \quad (8)$$

The parameter $\lambda \in [0, 1]$ modulates the trade-off, and $\mathcal{P}_{\text{UAV}}$ denotes the corrected UAV waypoint history. The first term in Eq. (8) quantifies the travel cost, normalized from $\frac{1}{2}$ to $\frac{3}{2}$ based on the fixed candidate radius. It penalizes inefficient detours from the current position to the estimated tag location. The second term quantifies the expected localization gain by evaluating the horizontal dilution of precision (HDOP) with the candidate included; lower HDOP indicates better geometric diversity and improved estimation convergence [40]. By combining these two objectives, the planner selects waypoints that ensure both efficient navigation and precise tag localization.

After selecting the waypoint p_{next} that minimizes Eq. (8), the UAV moves to that location, collects new UWB and INS measurements, and passes them to the joint optimization module for trajectory and tag estimation.

C. Mid-Flight Phase – Joint Optimization for Trajectory-and-Tag Refinement

To address the compounded errors from ambiguous drone positioning discussed in §III-C, this module jointly refines the corrected UAV trajectory and the estimated tag location. We define a cost function $\mathcal{J}(\hat{p}_{\text{UAV}}(\cdot), \hat{p}_{\text{tag}})$ that jointly evaluates the corrected UAV trajectory and the estimated tag position:

$$\mathcal{J} = \sum_t \left[\underbrace{\|\hat{p}_{\text{UAV}}(t) - p_{\text{INS}}(t)\|^2}_{\text{INS consistency}} + \alpha \cdot \underbrace{\left(\|\hat{p}_{\text{UAV}}(t) - \hat{p}_{\text{tag}}\| - D_{\text{UWB}}(t)\right)^2}_{\text{UWB distance matching}} \right] \quad (9)$$

The weighting factor α reflects the system's implicit balance between inertial consistency and range agreement. Directly solving Eq. (9) is intractable due to its non-convex structure. Instead, we perform alternating optimization via two substeps:

UAV Trajectory Correction. Given the tag estimate $\hat{p}^k_{\text{tag}}$ at the k-th iteration, we correct the UAV trajectory through translation-only updates. This formulation reflects a key limitation of single-anchor UWB localization: range constraints are radially informative but offer poor observability in the tangential direction. To enhance robustness and temporal smoothness, we apply an exponentially weighted moving average (EMA) to the velocity, as visualized in Fig. 7:

$$v_{\text{LPF}}(t) = \beta_t v_{\text{INS}}(t) + (1-\beta_t) v_{\text{LPF}}(t-1), \quad (10)$$

where the weight β_t is determined based on the consistency between the INS velocity and the UWB-derived radial velocity. We define the latter as:

$$v_{\text{UWB}}(t) = \frac{D_{\text{UWB}}(t) - D_{\text{UWB}}(t-1)}{\Delta t}, \tag{11}$$

where $D_{\text{UWB}}(t)$ denotes the measured distance at time t, and Δt is the sampling interval. The reliability score ρ_t and corresponding weight β_t are computed as:

$$\rho_t = \exp\left(-\frac{|v_{\text{UWB}}(t) - v_{\text{INS}}(t) \cdot u(t)|}{\delta}\right) \tag{12a}$$

$$\beta_t = \begin{cases} \max(\beta_{\text{base}} \cdot \rho_t,\ \beta_{\min}), & D_{\text{UWB}}(t), D_{\text{UWB}}(t-1) \text{ available} \\ \beta_{\text{raw}}, & \text{otherwise} \end{cases} \tag{12b}$$

where $u(t)$ is the unit vector from the UAV to the UWB anchor, δ controls the sensitivity of the reliability estimation, and β_{raw} is a fallback weight used when either $D_{\text{UWB}}(t)$ or $D_{\text{UWB}}(t-1)$ is unavailable. The EMA adaptively filters the INS trajectory using this reliability score, leveraging UWB's robustness against long-term drift.

Rather than relying on fixed global parameters, the reliability-related terms $\theta_j = \{\delta_j, \beta_{\text{base},j}, \beta_{\text{raw},j}\}$ are optimized independently for each trajectory segment using Bayesian optimization. The objective is to minimize the deviation between the corrected trajectory and a nominal reference path, linearly interpolated between the segment's endpoints. This unsupervised tuning without ground-truth labels enables the EMA filter to reconcile the UAV's measured motion with the intended straight-line trajectory, allowing the system to remain responsive to sensor dynamics while maintaining consistency with the planned path structure.

UWB Tag Estimation. After correcting the UAV trajectory, we re-estimate the tag position by minimizing the residual error across range observations:

$$\hat{p}_{\text{UWB}} = \arg\min_{p} \sum_{j} \left(\frac{1}{L_j} \sum_{t \in \mathcal{T}_j} \left(\|p - \hat{p}_{\text{UAV}}(t)\| - D_{3D}(t) \right)^2 \right) \tag{13}$$

where $\mathcal{T}_j$ denotes the index set of segment j, and L_j is the total 2D path length covered in that segment. This normalization mitigates the effect of redundant measurements in straight-line motion, which can amplify noise without improving observability. We solve this optimization using the ADAM optimizer [41] with velocity clipping to ensure stable convergence over noisy and non-convex residuals.

These two sub-steps are repeated until convergence:

$$\|\hat{p}^k_{\text{UWB}} - \hat{p}^{k-1}_{\text{UWB}}\| < \epsilon,$$

indicating that the tag position estimate has stabilized.

Once stabilized, the UAV evaluates the horizontal distance to the updated tag position. If this 2D distance falls below the predefined threshold D^{thr}_{2D}, the system transitions to the final phase for precise last-meter localization and delivery. Otherwise, the refined trajectory $\hat{p}_{\text{UAV}}$ and updated estimate $\hat{p}_{\text{UWB}}$ are passed to the DOP-based trajectory planning module to determine the next waypoint, forming a closed feedback loop.

D. Final Phase

Despite iterative refinements during the mid-flight phase, operating at high altitude amplifies the 3D-to-2D error propagation described in §III-D. To mitigate this, the UAV performs a *two-step descent* procedure, where each descent enables robust estimation of the horizontal distance $D^{(i)}_{2D}$ by leveraging 3D range measurements collected at different altitudes.

In the i-th descent step (i = 1, 2), the UAV descends from altitude H_i to $H_i + \Delta H$, with $\Delta H \approx -H/2$, where H is the UAV's initial altitude at the start of the descent sequence. Two 3D distances are recorded: $D^{(i,1)}_{3D}$ at altitude H_i, and $D^{(i,2)}_{3D}$ at $H_i + \Delta H$, satisfying:

$$\begin{aligned} {D^{(i,1)}_{3D}}^2 &= {D^{(i)}_{2D}}^2 + H_i^2, \\ {D^{(i,2)}_{3D}}^2 &= {D^{(i)}_{2D}}^2 + (H_i + \Delta H)^2, \end{aligned} \tag{14}$$

from which we derive:

$$H_i = \frac{{D^{(i,2)}_{3D}}^2 - {D^{(i,1)}_{3D}}^2 - (\Delta H)^2}{2\Delta H}, \quad D^{(i)}_{2D} = \sqrt{{D^{(i,1)}_{3D}}^2 - H_i^2}. \tag{15}$$

To improve robustness against measurement noise, each descent is divided into three vertical segments, and $D^{(i,1)}_{3D}$ and $D^{(i,2)}_{3D}$ are computed by averaging UWB readings from the first and last thirds, respectively. These averages correspond to altitudes near $H_i + \frac{1}{6}\Delta H$ and $H_i + \frac{5}{6}\Delta H$, reducing sensitivity to local disturbances.

After completing the first descent and estimating $D^{(1)}_{2D}$, the UAV performs a lateral maneuver of distance D_{final} and then conducts a second descent to obtain $D^{(2)}_{2D}$. These two measurements define intersecting circles in the 2D plane, yielding two candidate tag locations with identical range observations– a classic flip ambiguity. To improve disambiguation, the lateral maneuver is made orthogonal to the estimated tag direction, increasing spatial separation between candidates. The system evaluates both candidates using a mid-flight-derived loss function based on the UAV's full trajectory and range history, and selects the one with the lower residual as the final tag estimate. The UAV subsequently navigates to this location to complete the delivery.

V. Evaluation

We evaluate *NOVA* through both real-world experiments and simulations, focusing on localization accuracy, trajectory efficiency, and last-meter delivery performance.

A. Evaluation Setup

Implementation. We implement *NOVA* on the Argosdyne Aquila 3 platform [42], using the onboard telemetry system (argosALES) to monitor heading, velocity, and altitude (Fig. 8). As telemetry is accessible only via a proprietary GUI on this platform, OCR-based extraction is used to construct a real-time pseudo-INS as the primary motion reference throughout the flight; *NOVA* is otherwise agnostic to the telemetry interface.

A Raspberry Pi 4 onboard the UAV interface with a DWM-1001 UWB tag to collect distance measurements from a fixed

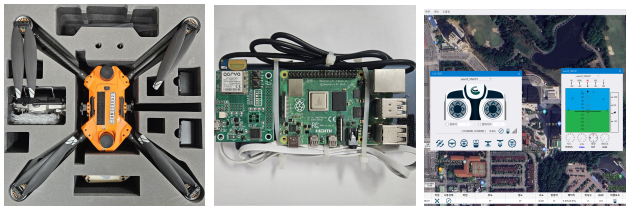

(a) Aquila 3 drone. **(b)** Raspberry Pi 4 with DWM1001 UWB tag. **(c)** argosALES dashboard for telemetry.

Fig. 8: Hardware and software components for implementation.

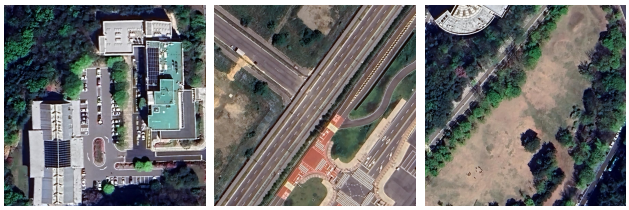

(a) Parking lot. **(b)** Wide road. **(c)** Park.

Fig. 9: Three experimental sites used for real-world validation.

anchor using Double-Sided Two-Way Ranging (DS-TWR), implemented via a modified Contiki-UWB example [43]. These measurements are transmitted to a ground server for centralized fusion with the pseudo-INS via a Python-based localization module, where iterative optimization is executed offboard, enabling real-time operation without computational burden on the UAV.

Experiment Setup. Flight tests are conducted in outdoor environments such as parks, parking lots, and roads shown in Fig. 9. Before each flight, the UWB tag's GPS location is approximated using a commercial smartphone to initialize navigation. While approaching the tag at an altitude of 30 m, the UAV switches to *NOVA* upon detecting UWB signals. Ground-truth trajectories are recorded via RTK-GPS (cm-level accuracy) only for offline verification. Table II summarizes key implementation parameters of *NOVA*, including sensing rates, filter settings, and optimization intervals.

Simulation Environment. We also developed a MATLAB simulator that models UAV dynamics, IMU outputs via the `IMUSensor`, UWB ranging, and barometric altitude sensing via the `altimeterSensor` module.[2] Table III lists the simulation parameters used throughout our evaluation. Each simulation result averages over 100 Monte Carlo trials for statistical robustness.

B. Real-World Performance

We conduct five trials per environment. Fig. 10 illustrates a representative trajectory generated by *NOVA* in the parking lot environment. Blue circles denote the UAV waypoints determined during flight, while red squares indicate the estimated UWB tag positions computed at each waypoint. The flight begins with an initial descent at waypoint ①, followed by a lateral movement toward waypoint ② that is perpendicular to the initial UWB tag position estimated via GPS. From waypoint ② to ⑦, the mid-flight phase refines the UWB tag estimate while simultaneously correcting the UAV's own position, enabling progressively improved localization as the UAV approaches the target. Once sufficiently close to the tag–based on the estimate at waypoint ⑦–the UAV initiates a two-step descent by moving laterally toward waypoint ⑧ and refining its estimate throughout. It then refines the tag position and navigates to waypoint ⑨, successfully reaching the precise tag location.

Fig. 11(a) presents the localization error at three key stages: the initial GPS measurement used for tag initialization, the result after the mid-flight phase, and the final navigation error after completion of *NOVA*. The initial GPS measurements exhibited large localization errors, particularly in altitude, with even the smallest error exceeding 6.15 m. This highlights the limitation of GPS-only initialization, demonstrating that accurate last-meter delivery is infeasible without additional correction. The mid-flight phase reduced the average vertical error to 0.51 m and lowered the total localization error to 3.21 m, 2.85 m, and 3.47 m in the park, parking lot, and wide road, respectively. Although mid-flight phase significantly improved accuracy, sub-meter localization remained challenging due to the geometric and measurement limitations discussed

[2]MathWorks, Simulate UAV Waypoint Following with Different Wind Conditions, UWB Ranging Using IEEE 802.15.4z, UWB Channel Model.

TABLE II: Key implementation parameters related to *NOVA*.

Parameter	Description	Value
Measurement Parameters		
v_{UAV}	Target speed of drone	1.0 m/s
INS interval	Time interval between INS measurements	0.5 s
UWB interval	Time interval between UWB measurements	0.1 s
UWB channel	UWB Channel for DS-TWR	1
Initial Phase		
D_{init}	2D movement	5 m
z_{init}	Z-altitude distance	1 m
Trajectory Planning		
N	Number of Trajectory Candidates	24
λ	Weight b/w DOP and normalized distance	0.7
Joint Optimization		
Max_{opt}	Maximum number of optimization steps	20
D_{2D}^{thr}	Threshold to descend	1.0 m
ϵ	Threshold to stop joint optimization	0.1 m
$\beta_{\min}$	Minimum weight for EMA filtering	0.15
Max_{ADAM}	Maximum iteration of ADAM	500
η	Learning rate of ADAM	0.1
$v_{\min}^{adam}$ / $v_{\max}^{adam}$	Minimum / Maximum velocity of ADAM	0.1 / 30.0
Descent		
d_{lat}	Lateral movement at descent	1 m

TABLE III: Key Simulation Parameters

Category	Parameter	Value
Flight	Flight Speed	1.0 m/s
	Wind Noise (XY/Z)	0.3 / 0.1 m/s
	Horizontal Init. Offset	$r \sim \mathcal{N}(5\,\text{m}, 2^2)$, $\theta \sim \mathcal{U}(0, 2\pi)$
	Vertical Init. Offset	Gaussian (μ=0, σ=5 m)
IMU	Sampling Interval	0.01 s
	Noise Density	500 $\mu g/\sqrt{\text{Hz}}$
	Bias Instability	3000 μg
	Random Walk	0.01 m/s$^2 \cdot \sqrt{\text{Hz}}$
Barometer	Sampling Interval	0.1 s
UWB	Sampling Interval	0.1 s
	Channel	2 (3.9936 GHz)
	Tx Power / Noise Floor	-14 dBm / -114 dBm

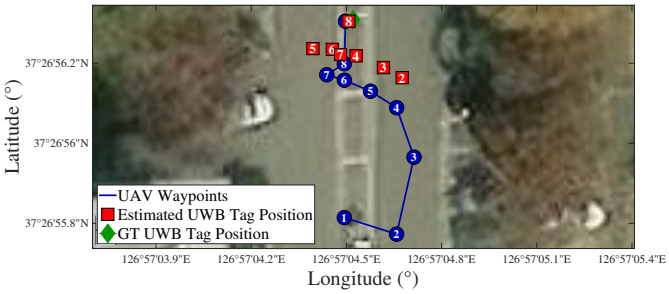

Fig. 10: Operation of *NOVA*– Bird's-eye view of UAV trajectory and estimated UWB tag position.

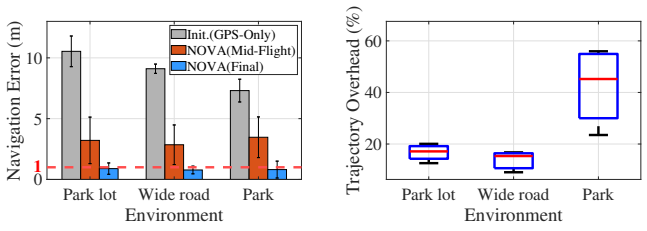

(a) Boxplot of navigation error. **(b)** Boxplot of trajectory overhead.

Fig. 11: End-to-end performance of *NOVA* under different environments.

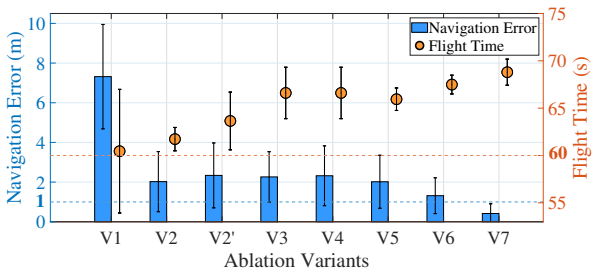

Fig. 12: Localization accuracy (blue, left axis) and flight time (orange, right axis) across ablation variants. Each bar shows the average over 100 trials; error bars denote standard deviation. Dotted lines indicate 1 m localization error and 60 s time benchmarks.

TABLE IV: Module configurations for each ablation variant.

Variant	Init. Flight	Trajectory Planning	Localization Method	Final Descent
V1	X	X	No Localization (1 m step)	X
V2	X	X	Multilateration (1 m step)	X
V2′	X	X	Multilateration (½-dist step)	X
V3	O	X	Multilateration (½-dist step)	X
V4	O	X	Joint Optimization	X
V5	O	O	Multilateration (½-dist step)	X
V6	O	O	Joint Optimization	X
V7 (NOVA)	**O**	**O**	**Joint Optimization**	**O**

in §III-D. The final-flight refinement reduced the average navigation error to 0.89 m (park), 0.81 m (parking lot), and 0.78 m (wide road), resulting in an overall average of 0.83 m. This final step resolved flip ambiguity and consistently enabled sub-meter accuracy in 12 out of 15 trials, with all navigation errors remaining below 1.6 m.

Despite the additional maneuvers introduced by *NOVA*, trajectory overhead – extra distance over ideal horizontal-vertical flight – remained modest in most environments (Fig. 11(b)). In both the parking lot and wide road scenarios, the average path length increased by less than 20%. In contrast, the park environment exhibited a higher overhead of 42.47% due to challenging UWB communication conditions under obstruction and environmental clutter, resulting in lower packet delivery ratio and delayed initial UWB detection. As a result, fixed-distance exploratory behavior during initial phase causes the UAV to traverse a wider area relative to its initial distance from the tag when UWB signals are detected at close range. This expanded coverage enhances geometric diversity, improves DOP conditions, and ultimately yields the highest localization accuracy among all trials. These results demonstrate that *NOVA* reliably achieves sub-meter navigation accuracy in real-world conditions with only modest flight overhead.

C. Simulation Performance

Fig. 12 presents the results of our ablation study comparing seven variants (V1-V7) of the *NOVA* framework in terms of localization accuracy (blue bars, left axis) and flight time (orange bars, right axis), with corresponding configurations detailed in Table IV. The "Localization Method" distinguishes whether the UAV updates its tag estimate using multilateration (at 1 m or ½-distance intervals) or performs joint optimization. V1 serves as a no-localization baseline, adjusting heading every 1 m based on the initial tag estimate. Compared to the baseline (7.32 m, 60.46 s), V2 introduces UWB-based multilateration at every meter, significantly reducing the error to 2.02 m, highlighting the importance of range-based correction. V2′ adopts a step-wise midpoint correction scheme, yielding comparable accuracy (2.34 m) with similar stability and slightly longer flight time (63.65 s), suggesting that sparse but structured updates can maintain performance while simplifying correction logic.

Adding an initial exploratory flight in V3 improves altitude observability but yields limited gain (2.26 m), suggesting that long-range geometric diversity alone is insufficient. Neither joint optimization alone (V4: 2.32 m) nor trajectory planning alone (V5: 2.02 m) achieves substantial improvement on its own–each addresses only part of the localization challenge. V4 suffers from poor convergence due to inadequate waypoint variation, while V5 cannot break the feedback loop between IMU drift and UWB noise (§III-C). V6, which integrates multiple enhancement modules, achieves a notable accuracy improvement (1.32 m) but remains limited by altitude-dominated errors (§III-D), which are overcome in *NOVA* (V7) through final descent, yielding sub-meter accuracy (0.42 m) with over 94% of the trajectory maintaining error below 1 m. These results indicate that isolated modules provide only partial benefit; effective performance requires their integration.

Fig. 13 compares the localization error time-series of *NOVA* against three baselines: Single Anchor (SA) [28], CKF-based Relative Positioning (RP) [32], and RP with realistic GPS error emulation (RP-Error). While RP also uses a cosine-similarity-based reliability metric similar to *NOVA*, it employs it solely to trigger Kalman filter updates, without influencing the fusion process itself. Unlike SA and RP, which assume perfect initialization, *NOVA* and RP-Error operate under realistic GPS errors Table III. All methods are evaluated over 10 trials using

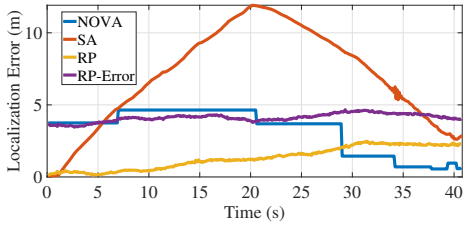

Fig. 13: Localization error over time in a single run.

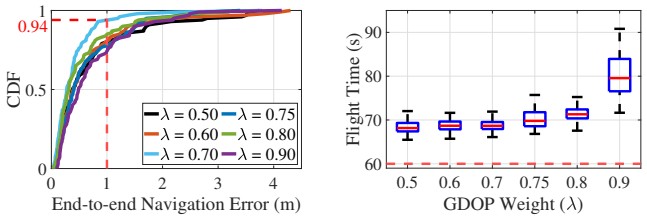

(a) eCDF of navigation error. **(b)** Boxplot of flight time.

Fig. 14: End-to-end performance of *NOVA* under different λ.

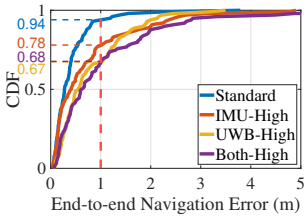

Fig. 15: Navigation error under different noise condition.

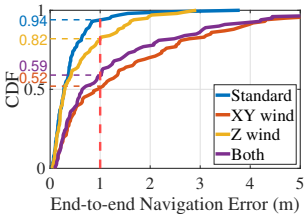

Fig. 16: Navigation error under different wind speed.

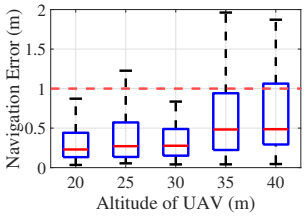

Fig. 17: Navigation error under different altitude.

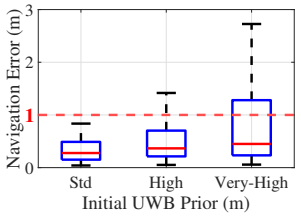

Fig. 18: Navigation error under different initial tag estimation.

a shared reference trajectory.

As shown in Fig. 13, SA exhibits mid-flight error spikes due to poor DOP but later improves, with a mean final error of 2.26 m. RP performs reliably with perfect initialization, yielding 1.27 m error–comparable to *NOVA* (1.26 m), despite *NOVA* starting from degraded initial conditions. In contrast, RP-Error fails to recover from initialization noise, resulting in the highest error (6.89 m) and highlighting the sensitivity of Kalman filter methods to initialization. *NOVA* consistently converges under realistic conditions, with its piecewise error curve reflecting discrete tag updates at planned intervals.

Fig. 14 illustrates the impact of varying DOP values on localization accuracy and flight duration. The empirical cumulative distribution (eCDF) in Fig. 14(a) shows peak accuracy at DOP = 0.7, achieving a final navigation error of 0.42 m, with 94% of the trajectory below 1 m. As shown in Fig. 14(b), flight time remains stable up to DOP = 0.7 but rises sharply beyond 0.75. Notably, lowering DOP below 0.7 yields little improvement, while increasing it past 0.75 leads to marginal accuracy gains at high time cost. These results suggest that a moderate DOP (around 0.7) provides the best trade-off between accuracy and efficiency.

We next evaluate the robustness of *NOVA* against internal sensor degradation and external wind disturbances. In Fig. 15, *IMU-High* doubles all IMU parameters (except sampling interval), while *UWB-High* raises the UWB noise floor from -114 dBm to -104 dBm. IMU degradation causes moderate impact (0.75 m average, 77% sub-meter), while UWB degradation had a more severe effect (0.81 m, 66%), confirming UWB quality as the dominant factor. *Both-High* yields the highest error (1.16 m) but a similar sub-meter rate (67%), and only IMU-degraded cases exhibit long-tail behavior, indicating that drift drives outlier failures. Fig. 16 tests robustness under wind disturbances with 2D and vertical wind modeled as zero-mean Gaussians with standard deviations of 0.35 m/s and 0.15 m/s, respectively–each 1.5× the typical ambient wind [44]. Sub-meter accuracy dropped from 94% (no wind) to 82% (*Z wind*) and 52–59% (*XY wind, Both*), with XY disturbances having the strongest effect on overall accuracy. Despite this, *NOVA* maintains mean errors of 1.665 m and 1.533 m under these harsh conditions, confirming its resilience against both sensor and environmental degradation.

Initial UAV–UWB conditions may affect localization accuracy. As shown in Fig. 17, increasing the final approach distance from 20 m to 40 m leads to a systematic drop in sub-meter success rate (from 94% to 74%), due to two compounded effects: degraded UWB ranging accuracy at longer distances, and vertical error amplification along the Z-axis as discussed in §III-D. Fig. 18 examines robustness to initial tag estimation errors under three perturbation levels: *Normal* ($r \sim \mathcal{N}(5, 2^2)$, $z \sim \mathcal{N}(0, 5^2)$), *High* ($r \sim \mathcal{N}(10, 5^2)$, $z \sim \mathcal{N}(0, 10^2)$), and *Very High* ($r \sim \mathcal{N}(20, 5^2)$, $z \sim \mathcal{N}(0, 20^2)$). Despite these challenging conditions, *NOVA* consistently achieves reliable convergence, with a mean final error of 0.94 m and 68% sub-meter success even under severe initialization errors.

VI. Conclusion

NOVA is a robust localization framework for UAVs operating with a single UWB anchor. Unlike conventional approaches that rely on accurate initialization or assume fixed trajectories with abundant geometric diversity, *NOVA* actively induces such diversity through segment-wise trajectory refinement and DOP-aware waypoint planning. By jointly optimizing the UAV's trajectory and anchor localization, *NOVA* achieves reliable performance even under ambiguous measurement geometries. Through both simulation and real-world experiments, we demonstrated that *NOVA* consistently delivers accurate localization across a range of practical scenarios, validating its effectiveness in dynamic and error-prone environments. Future work includes extending the method to multi-UAVs settings and applying it to large-scale field deployments.

References

[1] MarketsandMarkets, "Drone Package Delivery Market by Solution, Duration, Range, Package Size, Type, End Use, Region - Global Forecast to 2030," https://www.marketsandmarkets.com/Market-Reports/drone-package-delivery-market-10580366.html, 2024.

[2] Y. Yoo, J. Suh, D. Choi, J. Paek, and S. Bahk, "ASCEND: Altitude Selection for High-quality Cellular Connectivity on Drones," *IEEE Transactions on Vehicular Technology*, pp. 1–12, 2025.

[3] S. ur Rahman, G.-H. Kim, Y.-Z. Cho, and A. Khan, "Positioning of UAVs for throughput maximization in software-defined disaster area UAV communication networks," *Journal of Communications and Networks*, vol. 20, no. 5, pp. 452–463, 2018.

[4] S. Zieher, E. Olcay, K. Kefferpütz, B. Salamat, S. Olzem, G. Elsbacher, and H. Meeß, "Drones for automated parcel delivery: Use case identification and derivation of technical requirements," *Transportation Research Interdisciplinary Perspectives*, vol. 28, p. 101253, 2024.

[5] A. Cornell, B. Miller, and R. Riedel, "Solving the "Last-Meter" Challenge in Drone Delivery," https://www.mckinsey.com/industries/aerospace-and-defense/our-insights/future-air-mobility-blog/solving-the-last-meter-challenge-in-drone-delivery, 2023.

[6] T.-Y. Lo, J.-Y. Chang, T.-Z. Wei, P.-Y. Chen, S.-P. Huang, W.-T. Tsai, C.-Y. Liou, C.-C. Lin, and S.-G. Mao, "GPS-free wireless precise positioning system for automatic flying and landing application of shipborne unmanned aerial vehicle," *Sensors*, vol. 24, no. 2, 2024.

[7] D. Dissanayaka, T. R. Wanasinghe, O. De Silva, A. Jayasiri, and G. K. Mann, "Review of navigation methods for UAV-based parcel delivery," *IEEE Transactions on Automation Science and Engineering*, vol. 21, no. 1, pp. 1068–1082, 2023.

[8] W. Wang, L. Mottola, Y. He, J. Li, Y. Sun, S. Li, H. Jing, and Y. Wang, "Micnest: Long-range instant acoustic localization of drones in precise landing," in *Proceedings of the 20th ACM Conference on Embedded Networked Sensor Systems*, 2022, pp. 504–517.

[9] C. G. Grlj, N. Krznar, and M. Pranjić, "A decade of UAV docking stations: A brief overview of mobile and fixed landing platforms," *Drones*, vol. 6, no. 1, p. 17, 2022.

[10] Y.-J. Tu and S. Piramuthu, "Security and privacy risks in drone-based last mile delivery," *European Journal of Information Systems*, vol. 33, no. 5, pp. 617–630, 2024.

[11] S. S. Kannan, V. L. Venkatesh, R. K. Senthilkumaran, and B.-C. Min, "Upplied: Uav path planning for inspection through demonstration," in *IEEE/RSJ International Conference on Intelligent Robots and Systems (IROS)*, 2023, pp. 1126–1133.

[12] J. Park, G. Lee, J. Paek, and S. Bahk, "Cupid: Fast and Reliable Convergecast-Over-UWB Protocol for Dense Internet of Things," in *International Conference on Distributed Computing in Smart Systems and the Internet of Things (DCOSS-IoT)*, 2025, pp. 9–17.

[13] N. El-Sheimy and Y. Li, "Indoor navigation: State of the art and future trends," *Satellite Navigation*, vol. 2, no. 1, p. 7, 2021.

[14] Z. Liu, J. Liu, X. Xu, and K. Wu, "DeepGPS: Deep learning enhanced GPS positioning in urban canyons," *IEEE Transactions on Mobile Computing*, vol. 23, no. 1, pp. 376–392, 2022.

[15] J. G. Singla, "Examining quality of DGNSS derived positioning in data in urban city – A case study of an urban city in India," 2024. [Online]. Available: https://arxiv.org/abs/2411.19794

[16] L. Tavasci, F. Nex, and S. Gandolfi, "Reliability of Real-Time Kinematic (RTK) Positioning for Low-Cost Drones' Navigation across Global Navigation Satellite System (GNSS) Critical Environments," *Sensors*, vol. 24, no. 18, p. 6096, 2024.

[17] L. Zhao, W. Wang, Q. He, L. Yan, and X. Li, "Visual–Inertial Autonomous UAV Navigation in Complex Illumination and Highly Cluttered Under-Canopy Environments," *Drones*, vol. 9, no. 1, 2025.

[18] R. Wang and Z. Deng, "Rapid Initialization Method of Unmanned Aerial Vehicle Swarm Based on VIO-UWB in Satellite Denial Environment," *Drones*, vol. 8, no. 7, p. 339, 2024.

[19] J. Yang and S. Lee, "Ultrawideband coupled relative positioning algorithm applicable to flight controller for multidrone collaboration," *ETRI Journal*, vol. 45, no. 5, pp. 758–767, 2023.

[20] G. Ariante, S. Ponte, and G. Del Core, "Bluetooth low energy based technology for small UAS indoor positioning," in *IEEE 9th international workshop on metrology for AeroSpace*, 2022, pp. 113–118.

[21] W. Xue, W. Qiu, X. Hua, and K. Yu, "Improved Wi-Fi RSSI measurement for indoor localization," *IEEE Sensors Journal*, vol. 17, no. 7, pp. 2224–2230, 2017.

[22] M. Lam, L. Dodds, A. Eid, J. Hester, and F. Adib, "6D Self-Localization of Drones Using a Single Millimeter-Wave Backscatter Anchor," in *IEEE INFOCOM 2025 - IEEE Conference on Computer Communications*, 2025, pp. 1–10.

[23] M. Zhang, X. Xu, Y. Chen, and M. Li, "A lightweight and accurate localization algorithm using multiple inertial measurement units," *IEEE Robotics and Automation Letters*, vol. 5, no. 2, pp. 1508–1515, 2020.

[24] B. Yang, E. Yang, L. Yu, and C. Niu, "Ultrasonic-and IMU-based high-precision UAV localization for the low-cost autonomous inspection in oil and gas pressure vessels," *IEEE Transactions on Industrial Informatics*, vol. 19, no. 10, pp. 10 523–10 534, 2023.

[25] Y. Li, S. Zahran, Y. Zhuang, Z. Gao, Y. Luo, Z. He, L. Pei, R. Chen, and N. El-Sheimy, "IMU/magnetometer/barometer/mass-flow sensor integrated indoor quadrotor UAV localization with robust velocity updates," *Remote Sensing*, vol. 11, no. 7, p. 838, 2019.

[26] Z. Xiang, L. Chen, Q. Wu, J. Yang, X. Dai, and X. Xie, "An Improved UWB Indoor Positioning Approach for UAVs Based on the Dual-Anchor Model," *Sensors (Basel, Switzerland)*, vol. 25, no. 4, p. 1052, 2025.

[27] H. Luo, D. Zou, J. Li, A. Wang, L. Wang, Z. Yang, and G. Li, "Visual-inertial navigation assisted by a single UWB anchor with an unknown position," *Satellite Navigation*, vol. 6, no. 1, p. 1, 2025.

[28] X. Zhou, H. Zhong, H. Zhang, Y. Jiang, and Y. Wang, "Optimization-Based Single Anchor UWB Positioning System for Mobile Robots," *IEEE Transactions on Instrumentation and Measurement*, 2024.

[29] Y. Cao, C. Yang, R. Li, A. Knoll, and G. Beltrame, "Accurate position tracking with a single UWB anchor," in *IEEE international conference on robotics and automation (ICRA)*, 2020, pp. 2344–2350.

[30] B. Bao, C. Luo, Y. Hong, Z. Chen, and X. Fan, "High-Precision UAV Positioning Method Based on MLP Integrating UWB and IMU," *Tsinghua Science and Technology*, vol. 30, no. 3, pp. 1315–1328, 2024.

[31] Y. Wang, Q. Yang, H. Cui, and H. Fang, "Relative Localization With Non-Persistent Excitation Using UWB-IMU Measurements," *IEEE Transactions on Automation Science and Engineering*, 2024.

[32] Y. Lv, S. Liu, J. Dai, J. Li, and Y. Liu, "Improved CKF Collaborative Positioning Algorithm Between UAVs Based on UWB/IMU," *Measurement Science and Technology*, 2025.

[33] G. Brunner, B. Szebedy, S. Tanner, and R. Wattenhofer, "The urban last mile problem: Autonomous drone delivery to your balcony," in *International Conference on Unmanned Aircraft Systems*, 2019, pp. 1005–1012.

[34] A. Seth, A. James, E. Kuantama, S. Mukhopadhyay, and R. Han, "Drone high-rise aerial delivery with vertical grid screening," *Drones*, vol. 7, no. 5, p. 300, 2023.

[35] S. Xia, J. Guo, and C. Peng, "SSS: Towards Autonomous Drone Delivery to Your Door Over House-Aware Semantics," in *International Workshop on Mobile Computing Systems and Applications*, 2024, pp. 33–39.

[36] K. Park, J. Kang, Z. Arjmandi, M. Shahbazi, and G. Sohn, "Multilateration under flip ambiguity for UAV positioning using ultrawide-band," *ISPRS Annals of the Photogrammetry, Remote Sensing and Spatial Information Sciences*, vol. 1, pp. 317–323, 2020.

[37] C. Zhang, Z. Yang, H. Zhuo, L. Liao, X. Yang, T. Zhu, and G. Li, "A lightweight and drift-free fusion strategy for drone autonomous and safe navigation," *Drones*, vol. 7, no. 1, p. 34, 2023.

[38] A. Shastry and D. A. Paley, "UAV state and parameter estimation in wind using calibration trajectories optimized for observability," *IEEE Control Systems Letters*, vol. 5, no. 5, pp. 1801–1806, 2020.

[39] W. Suski, S. Banerjee, and A. Hoover, "System-level noise of an ultra-wideband tracking system," in *International Conference on Information Science, Signal Processing and their Applications (ISSPA)*, 2012.

[40] B. Li, A. G. Dempster, and J. Wang, "3d dops for positioning applications using range measurements," *Wireless sensor network*, vol. 3, no. 10, pp. 334–340, 2011.

[41] D. P. Kingma and J. Ba, "Adam: A method for stochastic optimization," *arXiv preprint arXiv:1412.6980*, 2014.

[42] Argosdyne Co., Ltd., "AQUILA-3 Product Page," https://argosdyne.com/kor/AQUILA-3F, 2025, accessed: 2025-07-29.

[43] P. Corbalán, T. Istomin, and G. P. Picco, "Poster: Enabling Contiki on Ultra-wideband Radios," in *International Conference on Embedded Wireless Systems and Networks (EWSN)*, 2018.

[44] T. Wetz, N. Wildmann, and F. Beyrich, "Distributed wind measurements with multiple quadrotor unmanned aerial vehicles in the atmospheric boundary layer," *Atmospheric Measurement Techniques*, vol. 14, pp. 3795–3814, 05 2021.